Assessing the Predictive Capability of Two-Phase Models for the Mechanical Behavior of Alumina/Epoxy Nanocomposites

G. M. Brown, F. Ellyin

Department of Mechanical Engineering, University of Alberta, Edmonton, Alberta, T6G 2G8, Canada

Received 30 October 2004; accepted 22 February 2005
DOI 10.1002/app.22188
Published online in Wiley InterScience (www.interscience.wiley.com).

ABSTRACT: A review of analytical modeling of particulate reinforcement is made as a prelude to the problem of microstructural inhomogeneity in nanocomposite materials. Noting the inevitability of dispersion nonuniformity, and variations in agglomerate morphology and filler-matrix interaction, the need to question the application of such models to novel materials arises. Employing the mechanical properties of alumina/epoxy nanocomposites, with known dispersion characteristics, an evaluation of the predictive capability of various models for Young's modulus, strength, and failure strain is made. Comparison between models is accompanied by a discussion of the parameters used in the fitting of macroscopic behavior to microstructural features.
 J Appl Polym Sci 98: 869–879, 2005

Key words: microstructure; modeling; nanocomposites; particle size distribution; structure-property relations

INTRODUCTION

With the advent of nanometer scale materials, particulate reinforcement of matrix materials has returned to the forefront of composite research, a place primarily occupied by composites of continuous fiber reinforcement. As reinforcing dimensions approach the molecular level, the interactions between particles and the relationship of reinforcement with surrounding matrix molecules can result in macroscopic behaviors potentially very different from those achieved with micrometer scale reinforcement.[1] Ceramic/plastic composites have benefited from these types of synergistic relationships, though the correct selection of constituent materials is necessary for chemical compatibility between phases to be achieved and favorable interactions above the molecular level promoted.[2]

However, many composite systems have chemical incompatibilities unsupportive of significant property gains, a problem inherent to the combination of alumina and epoxy. The design of composite components for use with each other can obviate many potential issues of concern; this has already been evidenced by carboxylate-alumoxanes[3] in nanocomposite synthesis, providing strength and stiffness improvements of 300 and 70%, respectively. Yet, it is to be noted that the majority of polymer nanocomposite systems do not have this advantage and specific processing techniques are consequently required to ensure the highest degree of homogeneity.

Indeed, ceramic powder incorporation with plastics can frequently have an opposing effect; for example, the high specific surface areas of these powders, which create the potential for macroscale homogeneity, also promote agglomeration and phase segregation processes—reducing dispersion and reinforcing efficiencies. Previous nanocomposite investigations have remarked on the presence of agglomerates and other forms of distribution nonuniformity. These cover thermoplastic matrices,[4,5] epoxies,[1,6] and other thermosets[7]; and carbon fibers,[5] silicates,[8,9] and inorganic oxides,[4,10] among others. For silica-based nanocomposites, the most advanced of polymer/ceramic nanocomposites, it is illustrative to note that "intercalation," "exfoliation," and "*in situ* polymerization" are all commonplace terms.[11] In other ceramic-plastic systems, analogues to these processes have been, or are currently being, developed with the aim of uniformly dispersing the ceramic and achieving a higher level of ceramic-polymer interaction. Until the efficacy of these processes is greatly improved, however, an expectation of some form of heterogeneity should exist.

BACKGROUND

In contrast to this expectation, the prediction and modeling of mechanical behavior typically assumes a macroscale material homogeneity, often with isotropy or orthotropy at the mesoscale. Two general approaches are employed. The earliest to be derived

Correspondence to: F. Ellyin (fernand.ellyin@ualberta.ca).

assumes the change in viscosity of a two-phase mixture parallels a change in other material properties, including elastic modulus. The second method models the two phase system as a representative volume element (RVE), with the response of the RVE to applied loads or displacements reflecting the average behavior of the system.[12] For macroscopically uniform materials these relatively simple models can be quite accurate in their prediction of the material behavior. Microscale parameters that alter the material behavior include the size, shape, and aspect ratio of the filler, as well as the distribution of the reinforcing phase in the matrix. These variables can be adjusted by the presence of third phase components, such as silane coupling agents, which have the capability to alter matrix-filler coupling and distributional statistics.[2]

From an experimental point of view, the ability to correlate macroscopically observed behavior with easily discernible parameters (i.e., component stiffness, volume fractions, etc.) is invaluable. Engineers of nanocomposite materials are employing the above-mentioned analytical techniques,[5,13,14] often with the "top-down" approach of discerning micrometer scale interactions from material behavior. Yet, a significant problem with such models is that simplicity and generality often provide predictions too widely bounded to be useful. And, as mentioned, significant gradients at the microstructural level can result from problems, such as dispersion nonuniformity. Consequently, macroscopic properties may be driven by limited regions of inhomogeneity (though this is more significant with respect to strength than modulus).

An evaluation of the predictive capability of such models, in the face of known micrometer scale inhomogeneity, is therefore of interest. In a previous investigation,[15] alumina/epoxy nanocomposites were synthesized with a spectrum of reinforcing distributions. It was shown that the mechanical properties were extensively influenced by the type and frequency of micrometer sized features. In this work, the techniques derived, using micro- and mesoscale reinforcement, are adopted for evaluation of the modeling capability of various analytical models, when applied to these nanocomposite materials. Furthermore, the extent to which these models can reflect the known distributional and morphological variations in reinforcing is evaluated for ultimate strength, failure strain, and tensile Young's modulus.

Modulus modeling

From an elasticity approach, the modulus of a composite material, E_c, has contributions from the matrix phase, E_m, and the filler or reinforcing phase, E_f. The extent of this contribution is determined in part by the volume fraction of the matrix, V_m and filler, V_f, as well as filler geometric orientation. The extreme bounds, between which all data should fall, are usually those derived from a strength-of-materials approach. The upper bound, known as the parallel model, assumes each phase is uniformly strained and no bonding between phases exists. It is most useful for continuous fiber reinforcement (i.e., 0° laminae).

$$E_c = E_m V_m + E_f V_f \tag{1}$$

The lower bound is the series model, which assumes that each phase is perfectly bonded to the other and both are equally stressed. This model is a more accurate description of 90° laminae or fillers that have been stratified into distinct layers. The series model is of the form

$$E_c = \frac{E_f E_m}{E_m V_f + E_f V_m} \tag{2}$$

Of course, a randomly distributed filler, even if uniformly distributed at a macroscopic level, should provide a modulus that falls between these bounds, either due to a variable degree of bonding between constituents or a multiplicity of locally "parallel" and "series" regions of filler within the composite. Hirsch[16] adopts this view and determines modulus as the sum of series and parallel components. The contribution of each type of reinforcing is determined by the fractions "x" and "1 − x," as shown in:

$$E_c = x(E_m V_m + E_f V_f) + (1 - x)\frac{E_f E_m}{E_m V_f + E_f V_m} \tag{3}$$

A more complete picture of linear elastic deformation is given by the model of Hashin and Shtrikman[17,18] (HS), as in eqs. (4)–(8)

$$E_c = \frac{9K_c G_c}{3K_c + G_c} \tag{4}$$

where, for the lower bound,

$$K_c = K_m + \frac{V_f}{1/(K_f - K_m) + 3V_m/(3K_m + 4G_m)} \tag{5}$$

$$G_c = G_m + \frac{V_f}{1/(G_f - G_m + [6V_m(K_m + 2G_m)]/[5G_m(3K_m + 4G_m)])} \tag{6}$$

and, for the upper bound,

$$K_c = K_f + \frac{V_m}{1/(K_m - K_f) + 3V_f/(3K_f + 4G_f)} \tag{7}$$

$$G_c = G_f + \frac{V_m}{1/(G_m - G_f + [6V_f(K_f + 2G_f)]/[5G_f(3K_f + 4G_f)])} \quad (8)$$

These are refined bounds for Young's modulus, which take into account Poisson's ratio contraction via the bulk modulus, with the composite as a whole considered isotropic. For rigid reinforcement, the HS predictions are widely spaced, owing to the large difference in the constituent moduli ($m = E_f/E_m \gg 1$). Here K_c, K_m, and K_f are the bulk moduli, and G_c, G_m, and G_f are the shear moduli of the composite, matrix, and filler, respectively.

The Paul model[19] assumes a cubic inclusion embedded in a cubic matrix, where the constituents are in a state of macroscopically homogeneous stress. It overpredicts the modulus at low filler fractions (though it comes closer to other models, as $V_f \to 1$). It is given as

$$E_c = E_m\left(\frac{1 + (m-1)V_f^{2/3}}{1 + (m-1)(V_f^{2/3} - V_f)}\right) \quad (9)$$

where, again, $m = E_f/E_m$.

In contrast to the previous models, the Cox model[5,20] assumes that the reinforcement consists of whiskers or short fibers, where contribution to the modulus is made in a manner similar to the rule of mixtures. An assumption of shear load transfer requires that the filler be of sufficient length for load transfer to occur. A transfer "efficiency" is incorporated to account for length and orientation variation by including the length to diameter ratio, "l/d" and an orientation factor, "q." While this model does begin to relate physical parameters to the macroscopically determined response, the need for shear transfer makes application of this model to nanocomposites difficult owing to less than critical length dimensions. However, inhomogeneity in distribution may permit the model a higher utility because of clumping in the micrometer range. The Cox model includes the matrix Poisson's ratio, ν_m, and is given as

$$E_c = E_m(1 - V_f) + q\left(1 - \frac{\tanh z}{z}\right)E_f V_f \quad (10)$$

where,

$$z = \frac{l}{d}\sqrt{\frac{E_m}{(1 + v_m)E_f \times \ln(\pi/4V_f)}}$$

Alteration of a polymer's modulus is accomplished by restriction of chain mobility and extensibility. As this is only effective within the proximity of the reinforcing phase, a high degree of dispersion is desirable. Included in this discussion are two types of models that take into account distribution nonuniformity: those based on the Einstein equation[21] and the Kerner equation.[22]

Einstein's model, eq. (11), is an approach based not on elasticity, but on the assumption that changes in the viscosity of a suspension can parallel changes in material properties, including elastic modulus. Hence, in the model given by

$$\eta_c = \eta_m(1 + K_E V_f) \quad (11)$$

η, the viscosity, might be replaced by G or E, as appropriate. K_E is the Einstein coefficient, also called the "intrinsic viscosity," which is a function of particle morphology and packing. K_E increases for increased filler aspect ratios ($l/d > 1$), and decreases slightly[21] for Poisson's ratios < 0.5. Equation (11) forms the basis for most models employing the viscosity approach.

Kerner's model, eq. (12), has been used in previous nanocomposite modeling[5,23] and is a commonly employed model owing to the dependence of modulus on agglomeration. The general form can be derived from the Halpin–Tsai equations,[24] with variations provided by Lewis and Nielsen[21] and McGee and McCullough.[25,26] The reduced form of the Kerner equation is

$$E_c = E_m\left(\frac{1 + ABV_f}{1 - B\psi V_f}\right) \quad (12)$$

incorporating the dependence on modulus with a variable "B," given as

$$B = \frac{E_f/E_m - 1}{E_f/E_m + A} \quad (13)$$

For spherical particles the constant A is given by

$$A = \frac{7 - 5v_m}{8 - 10v_m} \quad (14)$$

whereas for nonspherical particles, A is based on $A = K_E - 1$.

The Kerner equation includes the maximum packing that the given filler geometry can assume, ϕ_m, and a reduced concentration term, ψ, expressing the reduction in the influence of filler with increasingly high packing ability. Another way of looking at ϕ_m is the ratio of true filler volume to the volume the filler actually occupies. Table I provides example values of ϕ_m, for different particle geometries, and also approximate values of K_E. Agglomeration alters both ϕ_m, and therefore also ψ and K_E values; increased agglomeration causes a decrease in ϕ_m and an increase in K_E. ψ can be related to ϕ_m by a number of relations,[21] including

TABLE I
Maximum Packing Fractions and Einstein Coefficients for Particulate Reinforcement of Various Dispersion Geometries

Particles	Dispersion	Orientation to stress	ϕ_m	K_E
Spheres	Hex. close pack	Any. No slippage.	0.7405	2.50
	Random loose pack	Any. No slippage.	0.601	2.50
	Simple cubic	Any. Slippage.	0.5236	1.50
	Agglom. loose pack	Any. No slippage.	0.37†	$2.5/\phi_a$
Fibres	Uniaxially oriented	⊥ to tensile stress	0.820	1.50
	l/d = 4, 3-D random	Any.	0.625	≈ 3.2
	l/d = 8, 3-D random	Any.	0.480	≈ 4.8
	l/d = 16, 3-D random	Any.	0.300	≈ 10.2

All values taken from Nielsen,[42] except †, taken from Vassileva.[14] ϕ_a is the volume fraction of the spheres in a spherical agglomerate.

$$\psi = \frac{V_m}{\phi_m}[\phi_m V_f + (1 - \phi_m)V_m] \tag{15}$$

The Mooney[21] equation is one of the many derivatives of the Einstein equation. It has the form:

$$E_c = E_m \exp\left(\frac{K_E V_f}{1 - V_f/\phi_m}\right) \tag{16}$$

Again, ϕ_m is used, though sometimes the crowding factor, $S = 1/\phi_m$, is preferred. This relation has been modified for nonspherical particles by Brodnyan[16,27] to incorporate "p," the aspect ratio of the particle ($1 < p < 15$). Hence, eq. (16) becomes:

$$E_c/E_m = \exp\left(\frac{2.5V_f + 0.407(p-1)^{1.508}V_f}{1 - V_f/\phi_m}\right) \tag{17}$$

Perturbation of the stress/strain fields by particles increases the elastic energy required for deformation and consequently increases the elastic constant. Guth[28] incorporated this into the Einstein equation for spherical particles, eq. (18), and nonspherical particles, eq. (19):

$$E_c = E_m(1 + K_E V_f + 14.1V_f^2) \tag{18}$$

$$E_c = E_m(1 + 0.67pV_f + 1.62p^2V_f^2) \tag{19}$$

Strength modeling

Theoretically, as the reinforcing material approaches the scale of individual polymer chains, the ability to homogenize the composite increases. This permits a reduction in the potential flaw size associated with defects in the reinforcing itself, more complete wetting of the filler by the matrix, and the presence of smaller, void-like inclusions (forming at the contact points of different particles). The increasing interfacial area, associated with reducing the particle size, provides a more effective transfer of load, with enhanced bonding at the interface between matrix and filler. Additionally, the oft-present coupling agents also diffuse the interface, changing it into an interphase region (as filler and interphase will have comparable dimensions). Consequently, the filler will have a more extensive impact on the surrounding polymer chains, and the stress concentration created by the filler will decrease as a result of a reduction of gradient in material properties and a more effective transfer of loads from constituent to constituent.

However, the synthesis of nanocomposites frequently includes processing methodologies that preclude the creation of a homogeneous dispersion and result in the potential inclusion of flaw-like structures in the matrix. This becomes more likely the smaller the filler material, for accompanying the increased surface area of small particles is a greater propensity for aggregation. It should, therefore, be of little surprise that strength reduction is predicted for, and found with, particulate reinforcement. Incomplete penetration of the matrix into clumps, lower clump strengths, the presence of larger stress concentration features, and a reduced dispersion will, to some extent, result. All of these "realities" conflict with the potential benefits mentioned above and have often been the defining characteristics of micrometer scale reinforcement. A major limitation in the traditional approach to strength modeling is accounting for the actual mechanisms of load transfer and stress redistribution, and inclusion of physically oriented, rather than arbitrary, conceptual parameters.

The majority of two-phase models for the strength of particulate filled materials find their origin in the beliefs that the filler behaves as a stress concentrator and reduces the effective load carrying cross section of the matrix. Power law models are indicative of this,[12,16] neglecting any load transfer or interfacial characteristics and thus any contribution to the strength by the reinforcement. The general form of these equations is

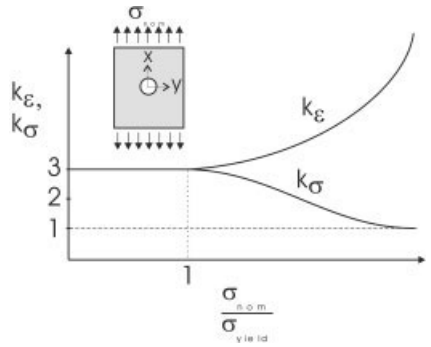

Figure 1 Uniaxial stress and strain concentration factors for a circular hole in a plate subjected to a nominal stress (or strain).

$$\sigma_c/\sigma_m = A - B(V_f)^n \tag{20}$$

where σ_c and σ_m are the ultimate tensile strengths of the composite and matrix. "A," "B," and "n" are all constants that describe particle shape and distribution. These predictions are best suited for materials with low filler-matrix interactions and for weak agglomerates, containing flaw or void-like regions.

At this point it would be useful to point out a term commonly employed in modeling that is used incorrectly. Although the intended meaning is obviously understood, the "stress concentration factor" is a misnomer for a modeling parameter that accounts for the effect of stress concentration. A comparable statement can be made for strain concentration. The stress and strain concentration factors can be defined as

$$k_\sigma = \frac{\sigma_{\max}}{\sigma_{\text{no min al}}} \quad \text{and} \quad k_\varepsilon = \frac{\varepsilon_{\max}}{\varepsilon_{\text{no min al}}} \tag{21}$$

As Figure 1 illustrates, these concentration factors are never less than unity. However, in the following description of strength modeling, a reduction in strength is predicted. The parameters used to account for the contribution of stress concentration to this reduction in strength have values less than 1 (i.e., see eqs. (22) and (25)). These parameters are, therefore, not the same as stress concentration factors.

For example, using a cubic particle embedded in a cubic matrix, Nielsen[29] introduced the stress concentration (strength reduction) parameter, k, where from eq. (20) k = A = B. In the absence of load transfer between constituents, they concluded that the matrix volume reduction necessitated the constant n = 2/3. This results in

$$\sigma_c/\sigma_m = k(1 - V_f^{2/3}) \tag{22}$$

Neglecting stress concentration, Nicolais and Narkis[30] similarly obtained:

$$\sigma_c/\sigma_m = 1 - 1.21V_f^{2/3} \tag{23}$$

though the inclusion of a variable maximum packing factor (in eq. (23) $\phi_m \approx 0.75$) gives the expression

$$\sigma_c/\sigma_m = 1 - \left(\frac{V_f}{\phi_m}\right)^{2/3} \tag{24}$$

In contrast, Piggott and Leidner[31] argued that a uniform distribution of a second phase is impractical except in theory. They included a parameter for stress concentration and additionally proposed the use of a constant for particle-matrix adhesion, "b," to give

$$\sigma_c = k\sigma_m - bV_f \tag{25}$$

Few two-phase models predict improvements in composite strength with rigid particle addition. Among these are the strength of materials approach, as given by the parallel model

$$\sigma_c = \sigma_m V_m + \sigma_f V_f \tag{26}$$

and adaptations of the Tsai–Hill[32,33] criterion. The latter has been employed for carbon fiber/thermoplastic nanocomposites,[5] though it is most aptly applied to long-fiber reinforcement and incorporates a knowledge of fiber length[34] (which may not be conceptually accurate at the nanoscale). Models that attempt to account for interfacial adhesion, thermal compressive stresses due to cure, and include frictional coefficients will not be considered here.

Strain modeling

Least developed are analytical models that pertain to failure strain. In the same vein that volume reduction of the matrix causes strength reduction, strain reduction follows from actual elongation experienced by the matrix increasing because of the volume occupied by the filler. The geometric relationship found below results:[29]

$$\varepsilon_c/\varepsilon_m = 1 - (V_f)^{1/3} \tag{27}$$

Modification of eq. (27) can be accomplished through the use of a parameter for strain concentration or by accounting for nonuniform distribution, as with strength modeling. This would provide an equation of the following form:

$$\varepsilon_c/\varepsilon_m = k[1 - (V_f/\phi_m)^{1/3}] \tag{28}$$

TABLE II
Explanation of Identifying Acronyms for Nanocomposite Series, Including a Summary of the Dispersion Quality and Extent of Alumina-Epoxy Interaction

Series	V_f (%)	Filler type	Surface treatment	Dispersion characteristics
S	2.92	spheres	- none -	small, weak and dispersed clumps; poor matrix integration
F	1.42	fibers	- none -	dispersed fibers; large, stronger aggregates; good matrix integration
F_L	2.12	fibers	- none -	dispersed fibers; very large, weak clumps; acceptable matrix integration
AF	0.72	fibers	APS	few dispersed fibers; large, cohesive, well integrated clumps
AF_{SS}	0.96	fibers	APS	range of clump sizes; dispersed fibers; diffuse boundaries; well integrated
GF	1.44	fibers	GPS	few dispersed fibers; large, cohesive, well integrated clumps

EXPERIMENTAL WORK

A detailed account of the synthesis, analysis of reinforcement distribution, and testing of nanoparticle alumina/epoxy composites is found in Brown and Ellyin.[35] A summary of the salient features of that work is now presented.

Partially hydrated alumina nanoparticles (Argonide Corp., USA), in the form of 80 nm average diameter spheres and 2–4 nm diameter, 50–100 nm long fibers were incorporated into an epoxy matrix (Epon 826/Epicure 9551; Resolution Performance Products, USA). The ceramic/polymer mixtures were mold-cast to create nanocomposite plates, from which modified dogbone specimens were machined.

Manipulation of the processing methodology produced a spectrum of alumina distributions, allowing comparison of the impact of dispersion and reinforcing uniformity on mechanical properties. Six nanocomposite specimens were produced. Series "S" incorporated spherical particles, uniformly dispersed in small clumps that contained voids and were poorly integrated with the matrix. Series "F" and "F_L" were pristine fiber nanocomposites containing both a well-dispersed and aggregated fraction of fibers, with the occasional large (> 40 μm) flocculation of fibers; the "L" in "F_L" designates the presence of an increased fraction of the large clumps. Three series of fiber nanocomposites containing silane surface modified alumina were created; all produced specimens with enhanced clump cohesiveness and improved fiber-matrix integration. A glycidyl-functional silane (3-glycidylpropyltrimethoxysilane, Aldrich 104884), designated "GPS," was employed for surface modification of one fiber batch used in "GF" series specimens. This series contained a reduced fraction of well dispersed alumina. A diamino-functional silane (3–2aminoethylaminopropyltrimethoxysilane, Aldrich 440167), or "APS," was used to treat two batches of fibers. Specimens containing these fibers are denoted "AF" and "AF_{SS}," where the "ss" subscript refers to a settling stratification process to reduce the fraction of clumps retained in the cast plate. For purposes of quick reference, Table II provides an overview of the series produced and the general nature of the alumina distribution in each.

Monotonic tensile and fracture tests were then conducted at room temperature. Analysis of particle size and shape distribution was made using TEMs of specimen cross sections, with fracture surfaces revealing the extent and type of filler/matrix interactions. An example comparison of the alumina dispersion in various series is provided in Figure 2.

Failure stress and strain were both taken at specimen failure and, in the absence of strain softening, represent ultimate strength and strain, respectively. The tensile Young's modulus was determined from the slope of a linear fit to 1% of the data, a compromise between secant and tangent moduli. Table III summarizes the experimental results of the tensile tests, with values representing the average of the results for each nanocomposite series. All data is normalized with respect to the average neat epoxy data.

COMPARISON OF MODELS WITH EXPERIMENTAL DATA

The constituent material properties used in all models are provided in Table IV. The definitive mechanical properties of the alumina are undetermined, owing to a paucity of data on nanoparticulate materials in general and this product specifically. Assumptions were made based on the information at hand[36] and gleaned from experiments[15]; all fall within the range of values provided in the literature.[37,38]

Modulus prediction

Establishing the plausibility of the experimental results is first made using the strength of materials and Hashin–Shtrikman (HS) bounds. Figure 3 presents the upper and lower bounds for each model, on a plot of normalized modulus versus volume fraction of alumina. Also included are experimental data and the Hirsch (H) model, eq. (3). For the latter, the fractions of parallel and series components (x and $1 - x$, respectively) are chosen to bracket the data. The experimental values all fall between the bounds of even the more conservative HS model, though the separation at this modulus ratio ($m \approx 146$) is too great to permit any predictive capability. The Hirsch model reveals that

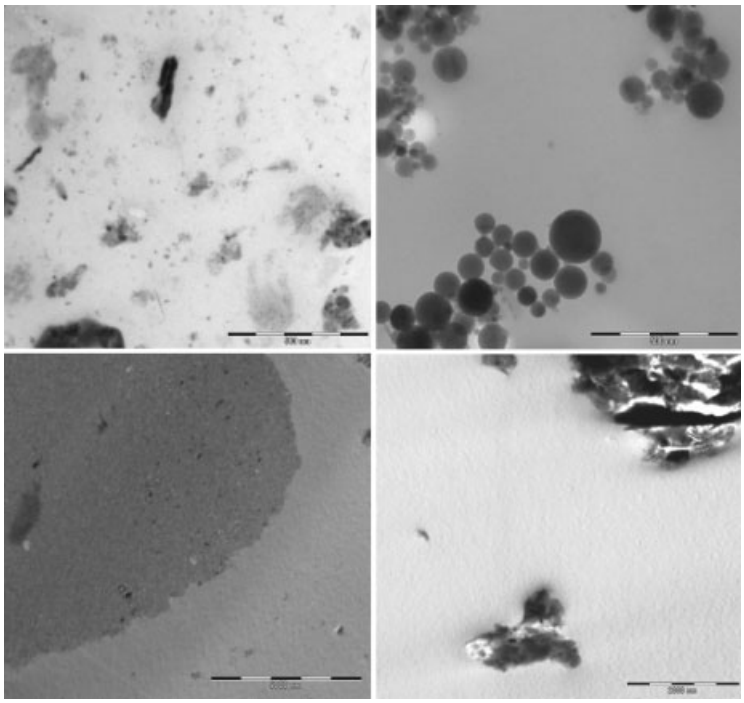

Figure 2 TEMs of nanocomposite specimens, illustrating the quality of the non-dispersed fraction of alumina. Clockwise from top left: Series AF_{SS}, bar = 500 nm; Series S, bar = 500 nm; Series GF, bar = 5000 nm; Series F_L, bar = 5000 nm.

the spread correlates to a difference in the fraction of parallel and series regions of 7%, with the main outliers being F series (at x = 9%) and S series (at x = 2%). F series specimens evidence a higher modulus, owing to the load carrying capacity of smaller, higher strength aggregates, with a large fraction of small fibers that can more extensively influence matrix deformation. In contrast, the lack of adhesion and weak clumping of S series specimens reduces the ability of the alumina to carry load and prevents modulus enhancement to the same extent as in the F series. Most interestingly, the proximity of the S series to the strength of the materials' lower bound would suggest a higher degree of bonding, though this is not seen at the microstructural level (i.e., refer to Fig. 2 and Table II).

TABLE III
Summary of the Tensile Mechanical Properties of Alumina/Epoxy Nanocomposites (all values normalized with respect to neat epoxy)

Series	V_f (%)	$E/E_{(epoxy)}$	$\sigma_f/\sigma_{f(epoxy)}$	$\varepsilon_f/\varepsilon_{f(epoxy)}$
Epoxy	-	1	1	1
S	2.92	1.13	0.88	0.36
F	1.42	1.19	0.98	0.48
F_L	2.12	1.15	0.89	0.40
AF	0.72	1.05	1.04	0.65
AF_{SS}	0.96	1.09	1.11	0.74
GF	1.44	1.09	1.03	0.65

The models of Paul, Cox, and Ishai and Cohen (I and C) are shown in Figure 4. The Paul model overestimates reinforcement at low filler volume fractions, though this should be expected with the assumption of perfect interfacial adhesion. The curve for eq. (9) reflects the enhanced modulus of F series specimens (an 8% overprediction), but cannot adequately model the poor bonding in S series specimens (a 35% overprediction). This is more intuitive than the series model prediction. Furthermore, adhesion enhancing agents like silanes are rarely present as monolayers and in the case of modulus can act as spring-like connections between constituents, moderating stiffening action. This is reflected in the moderate modulus enhancements of treated fiber series. In contrast, the uniform displacement case of Ishai and Cohen (I and C)[39] underestimates all of the data.

Two curves are shown in Figure 4 for the Cox model, each pertaining to an assumed l/d of 20. The upper is for a 2-D orientation factor of 1/2 and the lower uses q = 1/6. For monodispersed fiber reinforcement, an approximate l/d of 20 would be appropriate, though its applicability with shear transfer is questionable at this scale. A ratio of 3 would more accurately represent the geometry of reinforcement, though even assuming a 2-D random arrangement necessitates an l/d ratio of 25 to predict F series data. The knowledge that a fraction of well dispersed, high-aspect-ratio fibers is found should not permit the use of a higher l/d. This, in addition to the existence of a

TABLE IV
Properties of Constituent Materials Used in the Modeling of the Mechanical Behavior of Alumina/Epoxy Nanocomposites.

Mechanical property	Units	Epoxy†	Alumina	
			Theoretical‡	Assumed
Tensile modulus, E	GPa	2.57	355–396	375
Shear modulus, G	GPa	0.97	145–165	160
Bulk modulus, K	GPa	3.3	210–265	255
Poisson's ratio, ν	-	0.37	0.22–0.27	0.25
Density, ρ	kg/m^3	1150	3500–4000	3500
Ultimate strength, σ_{ult}	MPa	80	1000–2000	1400

† - values supplied by Resolution Performance Products,[36] except for ν from Hu,[43] and ρ and σ_{ult} from Brown and Ellyin[35];
‡ - values obtained from Harper.[38]

3-D random arrangement of fibers, suggests that the Cox model is conceptually unfit to approximate this data.

The curves for various derivatives of the Einstein equation are found in Figure 5. These models also incorporate l/d ratios (p), but additionally contain ϕ_m or K_E in a bid to account for the quality of distribution. Guth's model (G), eq. (19), brackets the data for p = 15 and p = 5 (dashed and broken lines), while Brodnyan's eq. (17) does the same for p = 9 and p = 3.5 (solid line, BN). Here, both models reflect the trend in the data of increasing modulus with a high fraction of high aspect ratio reinforcement, particularly Brodnyan's model at p = 3.5. While $\phi_m = 0.37$ is used, it is interesting to note that large variations in ϕ_m are possible at this low V_f without any appreciable variation in modulus.

The lowest curve is for spherical data, as modeled by Guth's eq. (18), with $K_E = 2.2$ and p = 1 (dot-dash line, G-s). It is almost identically the Mooney model, eq. (16), for $\phi_m = 0.37$, which is not shown. Both fall short of the S series, though provide a lower bound for the experimental data. Little can be directly elucidated from these models with respect to physical dimensions, though a general trend for clump geometry might be of some use (referring to the correlation between the lower bound and low p, and the higher bound and high p).

The most elaborate and adaptive prediction is offered by the Kerner equation, eq. (12), using the McGee[16] variation of the reduced concentration term, eq. (15), to account for a high modulus ratio and agglomeration. For the case of spherical particles, A is determined using eq. (14), with a ν_m of 0.37. For a random, loose packing of spheres, Table I suggests a ϕ_m of 0.601, though the presence of agglomeration should reduce this value; $\phi_m = 0.37$ has previously been employed by Vassileva and Friedrich.[14] This provides a lower bound for the data and agrees well with the presence of small, but evenly distributed, aggregates of spheres, as seen in the proximity of the curve to S series data in Figure 6 (solid, black line). For comparison, predictions (solid, gray curves) are provided for spherical particles having a loose packing ($\phi_m = 0.601$) and for an even greater degree of agglomeration, using $\phi_m = 0.25$. This latter ϕ_m corresponds more closely to the degree of clumping provided by the manufac-

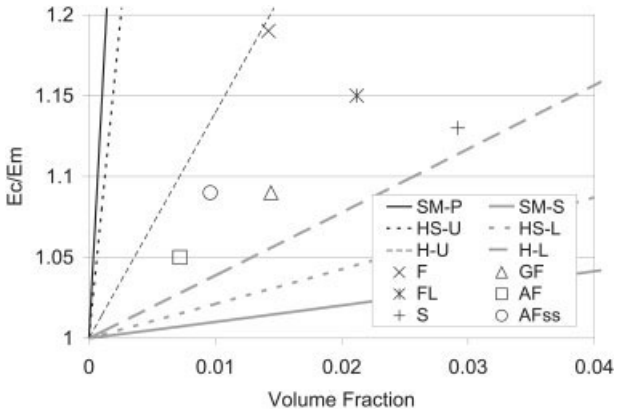

Figure 3 Strength of Materials (SM), Hashin–Shtrikman (HS), and Hirsch (H) model bounds for tensile Young's modulus. "U" and "L" are the upper and lower bounds; for H-U, x = 0.09, and for H-L, x = 0.02.

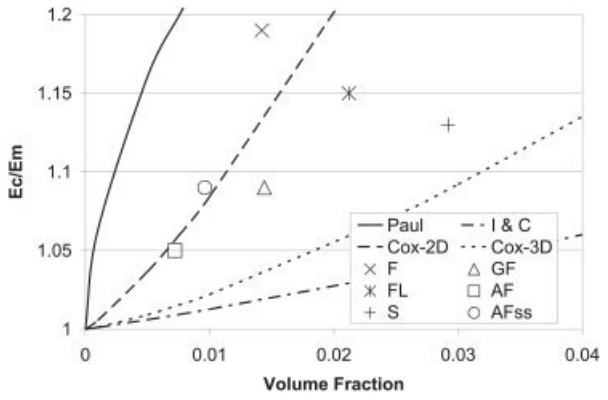

Figure 4 Tensile Young's modulus predictions for the Paul, Ishai and Cohen (I & C), and Cox models (2-D and 3-D), revealing a great spread in predictive capability.

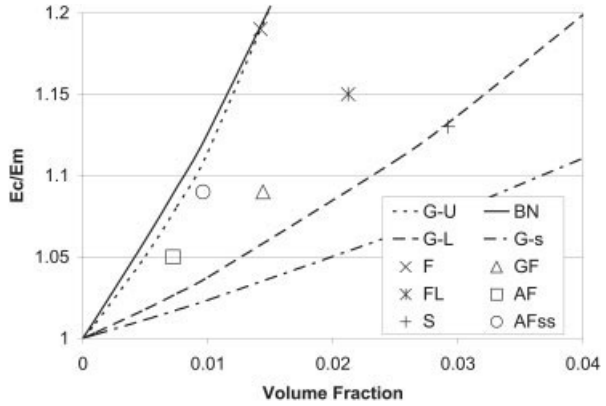

Figure 5 Comparison of predictive capabilities for models of tensile Young's modulus, having a basis in the Einstein equation. G-s is Guth's eq. (18) and is almost identical to Mooney's curve (eq. (16), not shown). G-U and G-L are Guth's eq. (19) with p = 15 and p = 5, respectively. BN denotes Brodnyan's model, using p = 3.5.

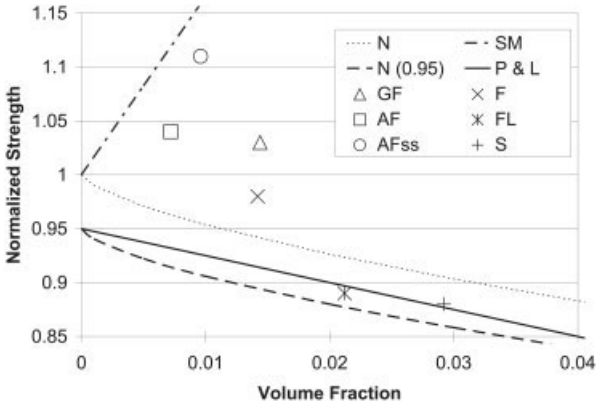

Figure 7 Comparison of predictions for ultimate strength of nanocomposite materials, outlining the utility of the power of law approach for modeling of untreated alumina reinforcement. N denotes Nielsen's models for k= 1 and k = 0.95. SM is for the strength of materials model. Piggott and Liedner's model is referred to by P & L.

turer[40] (the powder having a reduced bulk density, owing to clumps with ~ 75% void space). In fact, while the decrease from a random loose packing (ϕ_m = 0.601) is significant, Nielsen[21] suggests a slight increase in A, due to clumping, should similarly be included. This was not affected in this instance because of the weak nature of series S clumps, as discussed above.

Additionally, Figure 6 contains three curves for elongated, fiber reinforcement (broken, black lines), with an assumed maximum packing of ϕ_m = 0.37. "A" is found using $A = K_{E,mod} - 1$, where $K_{E,mod}$ is the Einstein coefficient at a chosen l/d, when adjusted for a ν_m = 0.37 (see Table I). The three l/d values used are 3, 8, and 16; the majority of agglomerates have an l/d ≤ 3, and 16 can approximate the monodispersed, high aspect ratio fiber case. Figure 6 shows that the curve for l/d = 3 falls in the middle of the data, in support of the observed agglomerate morphology. F_L, and particularly the silane treated fiber series, all have a marked increase in the fraction of fibers found in clumps; silane treated fiber series clumps also have increasingly ellipsoidal cross sections (higher l/d's). In contrast, the closest approximation for the F series incorporates a ϕ_m = 0.37 and an l/d of 8. However, this could equally be achieved with a ϕ_m of 0.15 and an l/d of 3 (not shown), suggesting a higher degree of agglomeration and a lesser contribution from the distributed fraction of fibers. The significance of the Kerner equation to predictions involving known micrometer scale inhomogeneity lies in the strong dependence on ϕ_m and ψ. By employing scaling parameters with a physical significance, this model can account for different fractions of fine alumina and the presence of aggregates of micrometer dimension more accurately than other models.

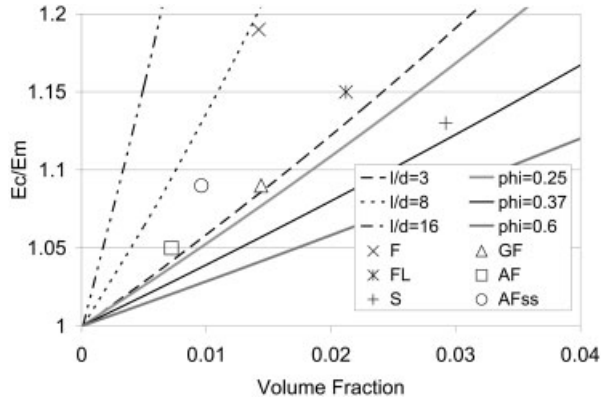

Figure 6 Kerner equation predictions for tensile Young's modulus evidencing strong dependence on ϕ_m and l/d, and closer ties to physical parameters of alumina dispersion. Black lines are for ϕ_m = 0.37; solid lines are for spherical particles (p = 1) of different maximum packing factors.

Strength prediction

Figures 7 and 8 reveal the two diverging trends indicated by the experimental data. The first is a decrease in strength, with increasing V_f, for the untreated alumina series. The brittle aspect of the epoxy matrix is emphasized by the presence of low levels of bonding and defective clumps. Well bonded and distributed fibers can carry the load otherwise taken by the matrix and enhance strength. The interaction of these two phenomena likely provides the overall behavior of the nanocomposites. For example, F series specimens have finely distributed fibers, that likely counterbalance the presence of larger clumps to a much greater extent than in F_L specimens, causing far less strength reduction. On the other hand, poor bonding of matrix

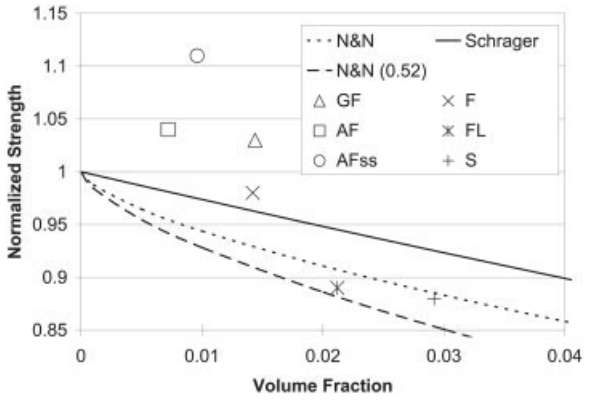

Figure 8 Further strength modeling, including the model of Schrager. Those of Nicolais and Narkis are denoted with N&N for eq. (23) and eq. (24), with $\phi_m = 0.52$ (brackets).

to S series particles allows little load transfer and consequently a strength reduction. Figure 2 illustrates the differences in microstructure that are reflected in the strength behavior.

Nielsen's model (N), shown in Figure 7, splits the data with a parameter for "stress concentration" of k = 1.0. To bracket the data on the low side requires a k value of 0.95, using the 2/3 power law (dashed line). The value of 0.5, as suggested by the author, is far too low. Similar to the Nielsen model, that of Piggott and Leidner (P and L) approximates the highest V_f data with a low parameter for "stress concentration" and low adhesion (k = 0.95, b = 2; solid line). Using eq. (25), it is difficult to approach the F series data point (×), without a negligible constant for strength reduction or a negative adhesion factor; the former is incongruous with the F_L series, and the negative b results in strength enhancement at higher V_f, unmerited with the given alumina distribution.

In Figure 8, the model of Nicolais and Narkis (NN) closely approximates F_L and S series specimens. This is done without accounting for stress concentration, though the model overestimates strength reduction for the F series, perhaps owing to the multimodal size distribution of fibers and clumps. This is the standard approximation, with ϕ_m set to 0.75—far too high for the known dispersion. A second curve is shown for $\phi_m = 0.52$, underestimating the failure stress while still not illustrative of the true state of agglomeration ($\phi_m \leq 0.37$). Also shown in Figure 8 is the Schrager model,[41] which provides the closest approximation to the F series, using an interfacial factor of r = 2.66. Decreasing this interfacial factor allows closer prediction of F_L and S series data.

An opposite trend to that predicted by the above models is found for silane modified alumina. This strength enhancement is modeled by the strength of materials approach, but only in a general manner, as it over-predicts all of the data. Figure 8 illustrates this. Again, the behavior is likely the sum of multiple mechanisms, with the silane enhancing adhesion and load transfer, and both broadening and diffusing the influence of the alumina. The inability of current thinking to account for this behavior is a great limitation when materials of this type are being introduced. Perhaps the most useful approach to modeling, in the face of such widely varied reinforcing sizes and matrix/filler interactions, is to account for the influence of different segments of the alumina population according to statistical considerations.

Strain prediction

Lastly, while predicting strength enhancements for particulate reinforcement is ineffective using simple, two-phase models, the modeling of strain response by analytical means is simply underdeveloped. Figure 9 portrays the failure strain response of the different nanocomposite series as a function of volume fraction. The main model for strain prediction is depicted by a solid curve, eq. (27). This model over-predicts failure strain, coming closer only for AF_{SS} data. It is apparent that the belief expressed by Nielsen, that a large strain reduction would correlate better with enhanced adhesion,[21] is not borne out by the data, with the weakest adhesion causing the lowest failure strains and the best adhesion, the highest. Including a parameter to account for "strain concentration" ($k = k_\varepsilon = 0.60$), in the same manner as for stress concentration, provides a better prediction of untreated alumina series properties. Yet, the trend given by this curve (solid, gray line) drastically under predicts the surface modified series, while providing for little further strain reduction at higher alumina volume fractions. More reflective of alumina distribution is to use eq. (28), with $\phi_m = 0.37$ for the treated alumina series and $\phi_m = 0.1$ for

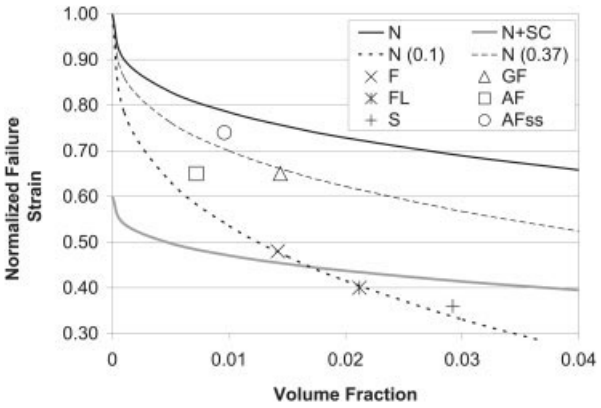

Figure 9 Modeling of strain reduction in alumina/epoxy nanocomposites using Nielsen's approach, denoted with an N. Variations are made using a parameter for a strain concentration, k = 0.6 (SC), and maximum packing fractions of $\phi_m = (0.1)$ and $\phi_m = (0.37)$.

untreated alumina. Both are shown in Figure 9, as a dashed and a dotted line, respectively.

CONCLUSIONS

Extensive application of relatively simple analytical models has been made in an effort to determine their applicability in the prediction of nanocomposite behavior. For the most part, only a general trend can be elucidated, and fitting of the models to the experimental data is typically bereft of physical intuition. This is particularly true of strength prediction, where the increased failure stress of nanocomposite series containing silane modified powders causes a mechanical behavior diverging greatly from traditional thought. On the other hand, applying the traditional models to materials with micrometer features of known defect shows much better correlation.

The most effective accounting of microstructural inhomogeneity lies in the maximum packing fraction, providing a straightforward and physically apt measure of agglomeration. The Kerner equation and a new use of the maximum packing fraction in strain modeling evidence the most support for this. In all cases, the link between known dispersion and parameter fitting is weak, and exacerbated by the great spectrum of reinforcing types associated with the nanometer scale filler. This range in the scale of alumina fiber reinforcement, as well as the interphase region of the silane treatment, must be accounted for in future modeling.

This work was funded in part by the National Science and Engineering Research Council (NSERC) of Canada. The authors would like to acknowledge the insight and advice provided by Dr. Zihui Xia and the members of the ACME group.

References

1. Wetzel, B; Haupert, F.; Zhang, M. Q. Compos Sci Technol 2003, 63 2055.
2. Kickelbick, G. Prog Polym Sci 2003, 28, 83.
3. Vogelson, C. T.; Koide, Y.; Alemany, Y. B.; Barron, A. R. Chem Mater 2000, 12, 795.
4. Ash, B. J; Stone, J; Rogers, D. F.; Schadler, L. S.; Siegel, R. W.; Benicewicz, B. C.; Apple, T.; In Filled and Nanocomposite Polymer Materials, Vol. 661, Section KK2.10; Warrendale, PA 2001. Mater Res Soc Symp Proc.
5. Tibbetts, G. G.; McHugh, J. J. J Mater Res 1999, 14, 2871.
6. Singh, R. P.; Zhang, M.; Chan, D. J Mater Sci 2002, 37, 781.
7. Cao, Y. M.; Sun, J.; Yu, D. H. J Appl Polym Sci 2002, 83, 70.
8. Eckel, D. F.; Balogh, M. P.; Fasulo, P. D.; Rodgers, W. R. J Appl Polym Sci 2004, 93, 1110.
9. Liu, T.; Tjiu, W. C.; Tong, Y.; He, C.; Goh, S. S.; Chung, T. J Appl Polym Sci 2002, 94, 1236.
10. Wei, B. Y.; Ho, S. L.; Chen, F. Y.; Lin, H. M. Surf Coat Technol 2003, 166, 1.
11. Alexandre, M.; Dubois, P. Mater Sci Eng 2000, 28, 1.
12. Farber, J. N.; Farris, F. J. J Appl Polym Sci 1987, 34, 2093.
13. Brechet, Y.; Cavaille, J. Y.; Chabert, E.; Chazeau, L.; Denievel, R.; Flandin, L.; Gauthier, C. Advanced Engineering Materials 2001, 3, 571.
14. Vassileva, E.; Friedrich, K. J Appl Polym Sci 2003, 89, 3774.
15. Brown, G. M. Master's Thesis, University of Alberta, Edmonton, Alberta, 2004.
16. Ahmed, S.; Jones, F. R. J Mater Sci 1990, 25, 4933.
17. Gol'dman, A. Y. Prediction of the Deformation Properties of Polymeric and Composite Materials (English Translation); American Chem Society: Washington: DC, 1994.
18. Hashin, H.; Shtrikman, S. J Mech Phys Solids 1963, 11, 127.
19. Paul, B. Transactions of the American Institute of Mechanical Engineering 1960, 36, 218.
20. Cox, H. L. Br J Appl Phys 1952, 3, 72.
21. Nielsen, L. E. Mechanical Properties of Polymers and Composites; Marcel Dekker: New York, 1974; Vol. 2, pp 379–415.
22. Kerner, E. H. Proc R Soc London 1956, 69B, 807.
23. Zeng, J; Saltysiak, B.; Johnson, W. S.; Schiraldi, D. A.; Kumar, S. Compos B 2004, 35, 173.
24. Halpin, J. C.; Kardos, J. L. Polym Eng Sci 1976, 16, 344.
25. McGee, S.; McCullough, R. L. Polym Compos 1981, 2, 149.
26. Munson-McGee, S. H.; McCullough, R. L. Polym Eng Sci 1994, 34, 361.
27. Brodnyan, J. G. Trans Soc Rheol 1959, 3, 61.
28. Guth, E. J Appl Phys 1945, 16, 20.
29. Nielsen, L. E. J Appl Polym Sci 1966, 10, 97.
30. Nicolais, L.; Narkis, M. Polym Eng Sci 1971, 11, 194.
31. Piggott, M. R.; Leidner, J. J Appl Polym Sci 1974, 18, 1619.
32. Hill, R. J Mech Phys Solids 1963, 11, 357.
33. Hill, R. J Mech Phys Solids 1963, 13, 213.
34. Hill, R. J Mech Phys Solids 1964, 12, 199.
35. Brown, G. M.; Ellyin, F.; Mechanical Properties of Alumina/Epoxy Nanocomposites: Influence of Processing Induced Inhomogeneities. (In Preparation).
36. Resolution Performance Products. Resin System for Filament Winding and Rtm. www.resins.com, 2003.
37. Dorre, E.; Hubner, H. Alumina: Processing, Properties, and Applications. Springer–Verlag: Berlin, 1984.
38. Harper, C. A., Ed. Handbook of Ceramics, Glasses and Diamonds: Advanced Ceramics and Composites; McGraw Hill: New York, 2001; Chapter 4, pp 4.1–4.46.
39. Ishai, O.; Cohen, L. J. International J of Mechanical Sciences 1967, 9, 539.
40. Tepper, F. Nano size alumina fibers (pdf), 2001. Argonide Corporation document containing information on alumina fibres. On the internet at: www.argonide.com.
41. Fried, J. R. Polym Sci Technol; Prentice Hall: Upper Saddle River, NJ, 1995; pp 279–283.
42. Nielsen, L. E. Predicting the Properties of Mixtures: Mixture Rules in Science and Engineering; Marcel Dekker: New York, 1978; pp 49–72.
43. Hu, Y. Ph.D. Thesis, University of Alberta, Edmonton, Alberta, 2002.